PhotoATRP Induced Self-Assembly (PhotoATR-PISA) Enables Simplified Synthesis of Responsive Polymer Nanoparticles in One-Pot

Ali Shahrokhinia,[a] *Randall A. Scanga,*[a] *Priyanka Biswas,*[a] *James F. Reuther,*[a*]

[a] Department of Chemistry, University of Massachusetts Lowell, Lowell, MA

KEYWORDS: Polymerization induced self-assembly (PISA), Photo-induced atom transfer radical polymerization, Polymer Nanoparticles (NPs), Stimuli-responsiveness

Corresponding author: James_reuther@uml.edu

For Table of Contents Use Only

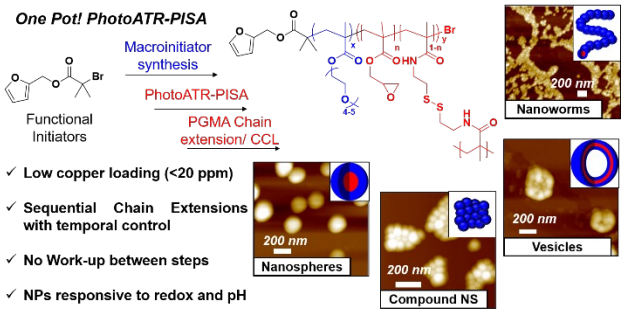

ABSTRACT: Photo-controlled atom transfer radical polymerization (PhotoATRP) was implemented, for the first time, to accomplish polymerization induced self-assembly (PISA)

mediated by UV light (λ = 365 nm) using ppm levels (ca. < 20 ppm) of copper catalyst at ambient temperature. Using $Cu^{II}Br_2$/tris(pyridin-2-ylmethyl)amine (TPMA) catalyst systems, PISA was per-formed all in one-pot starting from synthesis of solvophilic poly(oligo(ethylene oxide) methyl ether methacrylate) (POEGMA) blocks to core-crosslinked nanoparticles (NPs) utilizing poly(glycidyl methacrylate) (PGMA) and N,N-cystamine bismethacrylamide (CBMA) as the solvophobic copolymer and crosslinking agent, respectively. Sequential chain-extensions were performed for PGMA demonstrating capabilities for accessing multi-block copolymers with temporal control via switching the UV light on and off. Further, core-crosslinking of PISA nanoparticles was performed via the slow incorporation of the CBMA enabling one-pot crosslinking during the PISA process. Finally, the disulfide installed in the CBMA core-crosslinks allowed for the stimuli-triggered dissociation of nanoparticles using DL-dithiothreitol at acidic pH.

Introduction

The discovery of controlled/living radical polymerizations (CRP) has provided routes to precision polymers and copolymers with unprecedented level of structural, topological and chemical control. In recent years, PISA has emerged as a convenient method to synthesize different polymer nanoparticle (NP) morphologies in situ utilizing various CRP protocols.[1] In contrast to traditional self-assembly, typically limited to dilute solutions, PISA is achieved during the polymerization at much higher polymer/monomer concentrations (i.e. solid content) up to

50% w/w.[2] Theoretically, all CRP methods have potential for PISA applications including atom transfer radical polymerization (ATRP),[3] reversible addition-fragmentation chain transfer (RAFT)[4] and nitroxide-mediated polymerization (NMP).[5] However, study in this field has been mostly con-centrated on RAFT polymerization techniques due to the absence of the transition metal catalysts.

In recent years, CRP techniques mediated via photoirradiation have grown in popularity due to light's ease of administration, temporal and spatial control, and mild operating conditions.[6-10] Photo-initiated RAFT has been applied extensively to PISA allowing for control of polymerization mediated by different wavelengths of light ranging from UV to visible.[4, 11-14] With the exception of one recent report[15]; however, the solvophilic block is synthesized in homogenous media, and, after purification, is utilized as a macroinitiator for the block copolymerization of solvophobic blocks in selective solvents to form different NP morphologies in a second synthetic step.[16-18] Using this method the solid content and degrees of polymerization can be modulated to tune NP morphologies.[19-22] Further, to improve NP stability for biomedical applications, different strategies, such as core crosslinking (CCL) and shell crosslinking (SCL) procedures, are utilized, mostly via post-polymerization methods adding additional complications to synthetic protocols.[23-24]

The emergence of ATRP methods like Initiators for Continuous Activator Regeneration (ICAR) ATRP and Activators Regenerated by Electron Transfer (ARGET) ATRP allowed for

reduction of required catalyst concentration (~1600 ppm) and enhanced oxygen tolerance compared to conventional ATRP.[25-26] However, utilization of traditional radical initiators (e.g. AIBN) can affect end group incorporation limiting functionalization. Furthermore, the use of tin-based reducing agents offers further complications at limiting the metal species for potential biomedical applications. Despite these limitations, these techniques represent the only ATRP methods to be applied to PISA to date.[1, 26-27] Since these discoveries, recent advances in ATRP polymerizations have revealed the robust method of photo-induced ATRP (PhotoATRP). PhotoATRP has proven to be one of the most versatile and robust CRP protocols allowing for the one-pot synthesis of multi-block copolymers with high sequence fidelity.[6-7] This includes the unprecedented synthesis of multi-block copolymers with 23 different segments. When conducting these reactions in DMSO or trifluoroethanol, sequential chain extensions are possible even at high monomer conversions (ca. 98% conversion). Furthermore, this process can become "photo-controlled" at low copper loading providing temporal control allowing for the polymerization to be essentially turned on and off via toggling UV-irradiation.[28-30]

Herein, for the first time, we present a new PISA system based on PhotoATRP. The PhotoATR-PISA method described simplifies traditional PISA approaches via performing all synthetic steps, from solvophilic POEGMA macroinitiator synthesis to PISA to CCL of hydrophobic PGMA cores, in one-pot without any work-up between steps (Scheme 1). Further, this polymerization methodology is conducted with low copper catalyst concentrations (ca. $[CuBr_2]$ = 5 – 18 ppm) at ambient temperature. Additionally, we attempted multiple sequential

chain extensions of PGMA, tuning both PGMA degree of polymerization (DP) and solid content (%SC) in situ and opening the possibility for forming multi-block copolymers in PISA.

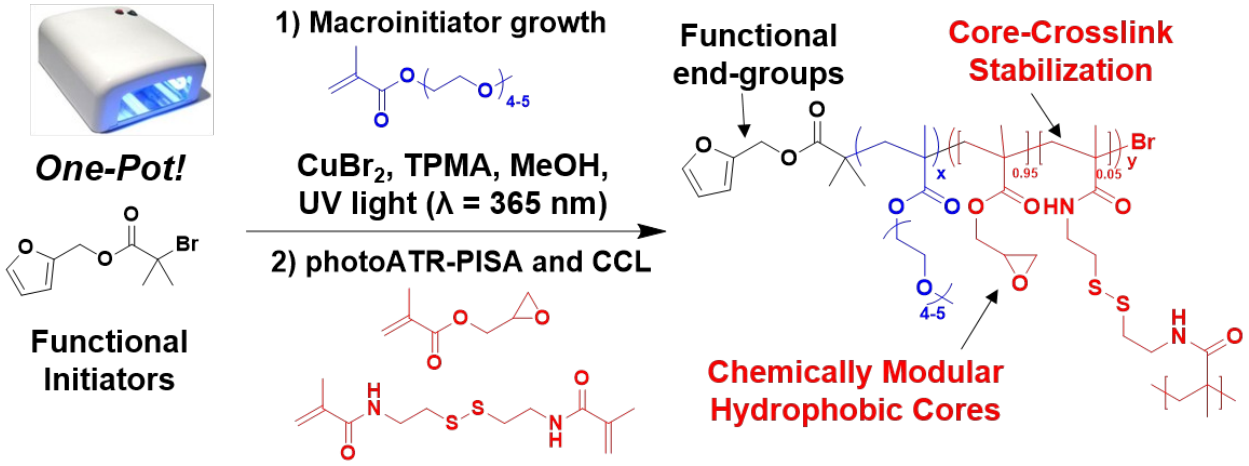

Scheme 1. The PhotoATR-PISA methodology allows for the one-pot synthesis of POEGMA macroinitiators, PISA formation of polymer NPs and covalent core-crosslinking of NPs in situ without any work-up between steps.

Materials and Methods

Materials- All solvents were purchased from Fisher Scientific and used as received. Cupric bromide ($Cu^{II}Br_2$, 99%, Sigma-Aldrich), Furfuryl alcohol (Sigma-Aldrich), triethylamine (Fisher Sci), 2-bromoisobutyryl bromide (Sigma-Aldrich), cystamine dihydrochloride (Sigma-Aldrich), methacryloyl chloride (Sigma-Aldrich), and Tris(pyridin-2-ylmethyl)amine (TPMA, TCI America) were used as received. For GPC, HPLC-grade THF was purchased from Fisher Scientific and used as received. Oligo(ethylene oxide)methyl ether methacrylate (OEGMA, M_n =

300 Da, Sigma-Aldrich) and glycidyl methacrylate (Alfa Aesar) were purchased and passed over a column of basic alumina to remove inhibitor prior to use.

One-pot PhotoATRP Induced Self-Assembly (PhotoATR-PISA)

Purified OEGMA monomer (1.0 mL, 3.5 mmol, targeted DP = 40), furan ATRP initiator (0.0875 mmol, 0.02153g), $Cu^{II}Br_2$ (0.4375 μmol, 97.8 μg), TPMA (1.75 μmol, 0.508 mg), DMF (internal standard; 27.1μl, 350 μmol) and the required amount of solvent according to the desired solid content were added to a septum sealed vial and degassed by purging with nitrogen for 45 min. Polymerization started via placing the degassed reaction mixture under the UV lamp and proceeded until 70% POEGMA conversion to preserve end group fidelity. Subsequently, monomer for the second block, GMA (7.53 mmol, 1.0 ml, targeted DP:86), was injected to the system after degassing for 15 min via a nitrogen purged syringe. The reaction proceeded under UV irradiation until the full GMA conversion for PISA and was terminated by exposing to air. Samples were taken periodically and analyzed using ^{1}H NMR and GPC analysis for kinetic analysis. Monomer conversion was calculated relative to internal standards (DMF; 10 mol% with respect to monomer).

Sequential PGMA Chain Extensions for one-pot PhotoATR-PISA

Purified OEGMA monomer (1 mL, 3.5 mmol, targeted DP:40), furan initiator (0.0875 mmol, 0.02153g), $Cu^{II}Br_2$ (0.4375 μmol, 97.8 μg), TPMA (1.75 μmol, 0.508 mg), DMF as an internal standard (27.1μl, 350 μmol) and the required amount of solvent according to the desired solid content were added to a septum sealed vial and degassed by purging with nitrogen for 45 min. Polymerization started via placing the degassed reaction mixture under UV irradiation and proceeded until ~ 70% OEGMA conversion to preserve chain end bromine fidelity.

Subsequently, GMA (7.53 mmol, 1.0 ml, targeted DP = 86) was injected to the system after degassing for 15 min via a nitrogen purged syringe. The mentioned procedure for the 2nd block was repeated and the reaction proceeded under UV irradiation until ~ 70% GMA conversion for the PISA in each addition. The mentioned procedure for the second block monomer addition continued until the the reaction was termination upon NP precipitation. In between each addition, the UV-light was switched off for a given period time stopping the polymerization. The UV-light was then turned on upon addition of N_2 degassed GMA monomer. Samples were taken periodically and analyzed using ^{1}H NMR, GPC, AFM, and DLS analysis in each addition for the core block.

In-situ CCL of PhotoATR-PISA NPs in one-pot and Nile Red Encapsulation

Following the procedure for one-pot PhotoATR-PISA, CBMA was added to with GMA monomer with the feed molar ratio of CBMA/(CBMA + GMA) = 0.05 and the reaction continued until the full GMA monomer and CBMA crosslinker conversion. Reaction aliquots were taken periodically and analyzed by AFM, DLS, GPC, and ^{1}H NMR. For Nile Red release experiments, Nile red (0.01 mol% with respect to GMA) was incorporated in the reaction media and was effectively encapsulated within NP cores. Dialysis against water was performed to remove the unencapsulated Nile red at the end of polymerization. These materials were then subjected to various protocols described below.

Nile Red Release through DTT Reduction of CCLs and Acidic Ring opening of Epoxides

To study the release behavior, 0.5 mL of reaction aliquot in water, containing Nile red loaded CCL NPs, were taken, split into 4 separate vials and diluted to 5.0 mg/ml. For two experiments, the solution pH was adjusted to pH = 4 upon titration with hydrochloric acid solution (0.6 M)

while two were maintained at pH = 7. To one CCL NP solution at pH = 4 and one at pH = 7, DTT was added as a redox trigger to disscociate disulfide CBMA crosslinks (c = 0.35 M). All 4 solutions were incubated and stirred at ambient temperature for 120 hours while the emission intensity changes at λ = 630 nm were monitored over different time intervals (Figure 5 in main text). Further, at different time intervals, DLS and AFM were performed to monitor the structure and integrity of CCL NPs over time.

Results and discussion

To incorporate functionality into our end groups, we synthesized furan-functionalized ATRP initiators via the esterification of 2-bromoisobutyryl bromide with furfuryl alcohol (Figure S1). These furan moieties will be utilized in subsequent reports. The POEGMA macroinitiator was synthesized by PhotoATRP in methanol (targeted DP = 40 for all PISA experiments), using $CuBr_2$/TPMA catalyst systems and commercial nail curing lamps as our UV source. For POEGMA macroinitiator synthesis, the polymerization was stopped (UV-light was switched off) at ~65 -70% monomer conversion to preserve the alkyl bromide chain end functionality. Without any work-up, PhotoATR-PISA was accomplished via gradient copolymerization of GMA from POEGMA macroinitiators (targeted DP(PGMA) = 86, 129, and 258; SC% = 25 and 32%). Attempted chain extensions at >80% conversion consistently resulted in poor reinitiation as evidenced by bimodal GPC traces following PISA (Figure S3). This has been observed previously when using methanol as a co-solvent in prior work.[6]

Screening the effect of $CuBr_2$ concentration on polymerization performance (Table 1) revealed enhanced control using low copper concentration (ca. [$CuBr_2$] = 5 - 18 ppm) and copper: ligand molar ratio of 1:4; as evidenced by the clean, unimodal shift toward the lower retention time after the chain extensions. In contrast, performing photoATRP at higher [$CuBr_2$] caused the polymerization to stall due to the excess deactivator in the system.[31] Additionally, the polymerization could not be reinitiated efficiently upon addition of GMA resulting in bimodal GPC traces (Figure S4).

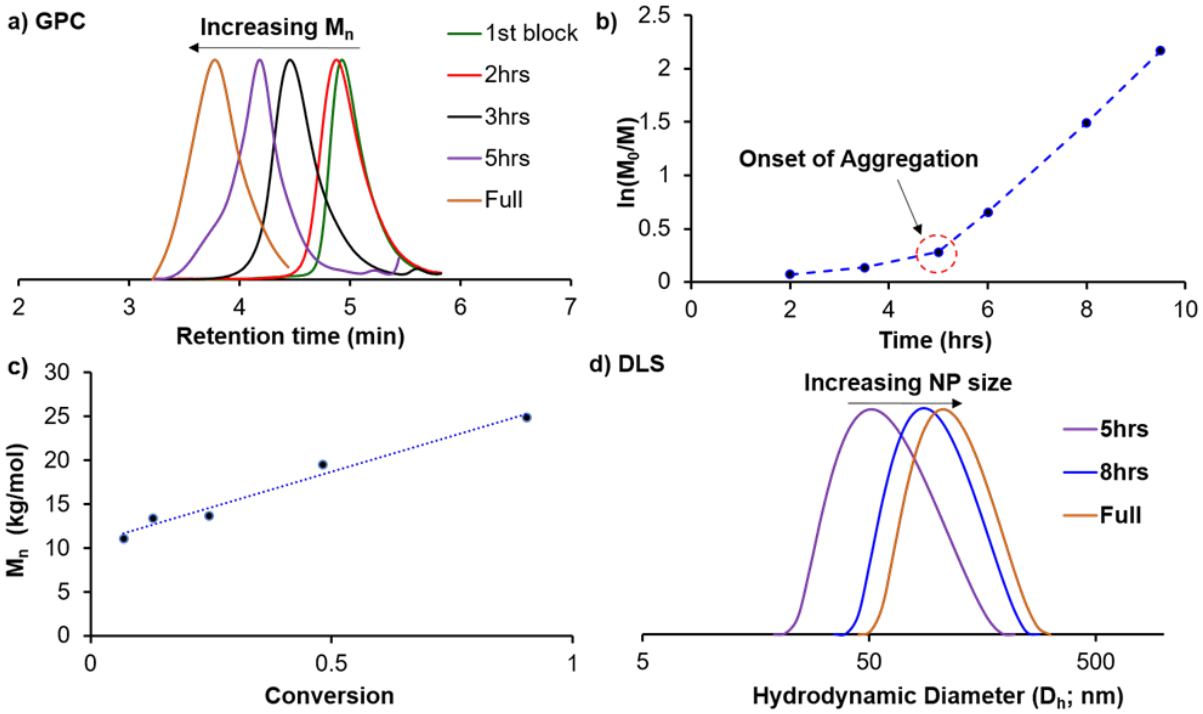

Figure 1. Kinetics of PhotoATR-PISA with a target DP(PGMA) = 129 and SC% = 25% showing clear shifts in retention time via GPC as GMA monomer is consumed (a); linear plots of ln(M0/M) vs. time (b) and Mn vs. conversion (c) were obtained, supporting CRP characteristics.

The increase in polymerization rate at ~5 h marks the onset of aggregation in PISA which is also evidenced by DLS showing increases in NP size as the polymer M_n continues to increase (d).

To demonstrate living polymerization control, the kinetics of photoATR-PISA was investigated utilizing our optimal copper concentration. As a model system, we first investigated PISA with a target DP(PGMA) = 129 and SC% = 25% (Figure 1). As GMA was consumed upon chain exten-sion, the molecular weight for the synthesized gradient copolymer increased in a unimodal form, an indication of controlled polymerization. Furthermore, the linear trend for the semilogarithmic kinetic plot (Figure 1b) confirms the expected pseudo-first order kinetics typical of CRP, albeit with one caveat. Similar to previous reports using RAFT-PISA,[4] the polymerization rate increased significantly after about 5 h which can be explained as the onset of aggregation. Upon aggregation, the GMA monomer migrates into the NP cores increasing the local concentration of monomer near propagating chain ends. The linear trend between M_n vs. conversion suggests chain transfer side reactions are suppressed, consistent with expectations (Figure 1c). Upon aggregation, we can observe increases in NP hydrodynamic diameter (D_h) by DLS from D_h = 42 nm to 102 nm as the polymerization proceeds and M_n continues to increase (Figure 1d).

To study the evolution of nanostructures formed, six one-pot PhotoATR-PISA experiments were conducted (Figure 2) utilizing POEGMA as the macroinitiator (DP = 32 – 40 as calculated by ^{1}H NMR); varying the target DP(PGMA) = 86, 129, and 258 at SC% = 25 w%

(PISA1, 3, and 5, respectively; Figure 2a and b) and 32 w% (PISA 2, 4, and 6, respectively; Figure 2c and d). The ^{1}H NMR spectrum of the POEGMA-grad-PGMA is shown in Figure S5 for PISA4 and remains consistent throughout all reactions confirming successful copolymer formation. Relying on the end group analysis utilizing the furan end group chemical shifts at 6.3 and 7.4 ppm, the final DP and M_n were calculated for the first block and the final copolymer and compared to GPC results. In all cases, GPC and NMR showed relatively good agreement with M_n(GPC) matching closely with theoretical M_n. Further, molecular weight dispersity (Đ) for final copolymers ranged from 1.35 – 2.10 at full monomer conversion, not uncommon for PISA methodologies (Table 1).

Table 1. PhotoATR-PISA characterization for DP(PGMA) = 86, 129 and 258, two different SC% = 25 (PISA1, 3 and 5, respectively) and 32% (PISA2, 4 and 6, respectively), and at different concentrations of $CuBr_2$.

Entry	**[OEGMA]:[Int]:[$CuBr_2$]:[TPMA]:[GMA]**	**M_n (kDa)[a] POEGMA**	**Đ [b] POEGMA[b]**	**M_n (kDa)[a] POEGMA-*grad*-PGMA**	**Đ [b] POEGMA-*grad*-PGMA**	**[$CuBr_2$] (ppm)**	**SC %**
1	40:1:0.005:0.02:86	9.9	1.29	23.6	1.34	9	25
PISA1	40:1:0.01:0.04:86	10.6	1.21	27.2	1.35	18	25
3	40:1:0.02:0.08:86	10.8	1.23	26.3	1.40	36	25
4	40:1:0.2:0.8:86	13.3	1.18	26.0	2.46	360	25
5	40:1:0.005:0.04:86	10.7	1.29	17.2	7.53	9	25
6	40:1:2:8:86	12.9	1.18	14.0	2.07	3600	25

PISA2	40:1:0.005:0.02:86	9.1	1.32	21.8	1.70	12	32
8	40:1:0.01:0.04:86	9.6	1.33	22.7	2.20	23	32
PISA3	40:1:0.005:0.02:129	9.0	1.30	30.6	1.90	7	25
PISA4	40:1:0.005:0.02:129	10.3	1.30	30.0	1.70	9	32
11	40:1:0.0025:0.01:258	8.7	1.32	32.0	5.70	2	25
PISA5	40:1:0.005:0.02:258	7.6	1.33	48.5	1.95	5	25
13	40:1:0.01:0.04:258	8.0	1.33	17.8	6.50	9	25
PISA6	40:1:0.01:0.04:258	9.8	1.28	46.9	2.10	12	32
15	40:1:0.04:0.16:258	9.7	1.31	62.2	2.60	46	32
16	40:1:0.08:0.32:258	10.5	1.32	40.4	3.55	92	32

a and b: Determined by GPC in THF, based on PS as calibration standards.

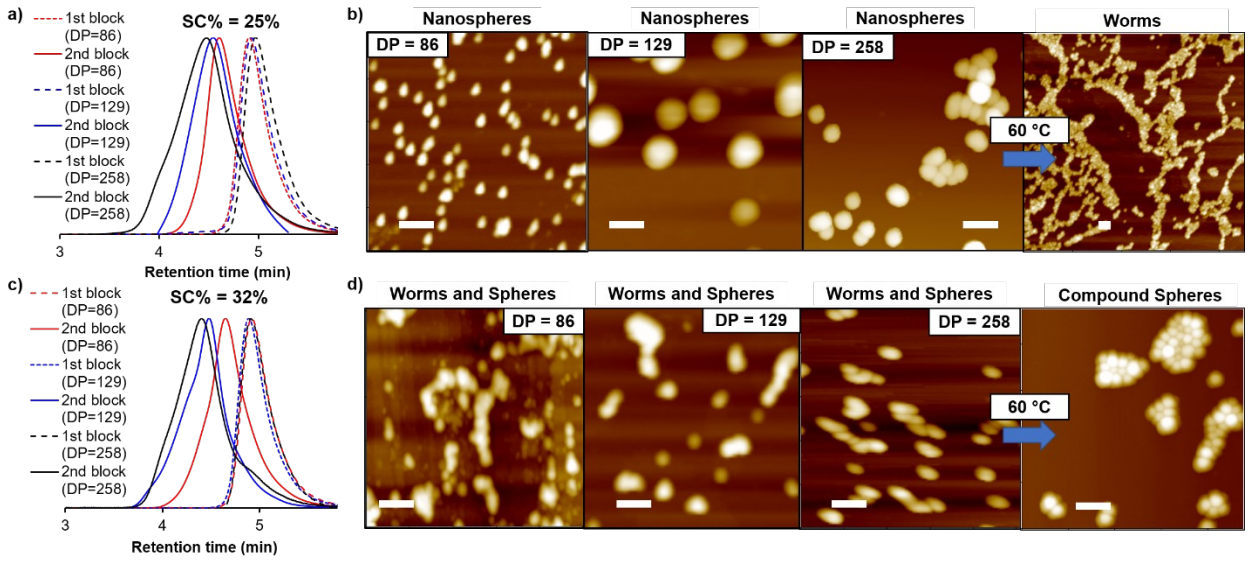

Figure 2. Attempted one-pot, PhotoATR-PISA experiments showing, via GPC, roughly the same starting M_n associated with POEGMA macroinitiator (a and c; dotted lines) utilized to target DP(PGMA) = 86, 129 and 258 (solid lines) and SC% = 25% (a and b) and 32% (c and d) to form self-assembled POEGMA-grad-PGMA NPs which were subsequently characterized using AFM (b and d) to reveal either nanospherical or mixtures of spherical and worm-like

micelle (white scale bars = 200 nm). Thermal annealing of aggregates with DP(PGMA) = 258 yielded morphological transitions to worm-like micelles and compound nanospheres for PISA 5 and 6, respectively.

The morphology evolution of PISA NPs was investigated by the AFM and DLS revealing that morphology was mostly influenced by SC% (Figure 2b and d; Table S1). According to DLS, increasing the DP(PGMA) led to increases in NP size for both solid contents increasing from D_h = 54 to 142 nm from PISA 1 to PISA5 at SC% = 25 % and D_h = 59 to 115 nm from PISA 2 to 6 at SC% = 32% (Figure S6). For SC% = 25%, mostly nanospheres were observed with dispersed nanospheres obtained at DP(PGMA) = 86 and 129 (i.e. PISA 1 and 3) while aggregated, compound nanospheres were observed at DP(PGMA) = 258 (PISA5). Sizes measured by AFM and calculated by DLS follow the same trend increasing as the DP(PGMA) increases and match closely in value and standard deviation (Table S1). At the higher SC% = 32%, mixtures of worm-like and spherical micelles were observed via AFM; considered an indication of the diffusion-limited aggregation and growth mechanism.[32] This kind of morphology is hypothesized to form via the collision and fusion between nanospheres upon aggregation, intensified at higher SC%. This hypothesis is supported by AFM showing clear linear association of nanospherical aggregates in the height profile of the micrograph (Figure 2d).

Unfortunately, none of the PISA samples synthesized provided higher order nanostructures such as vesicles or pure worm-like micelles. Since the polymerization was conducted at ambient temperature, we hypothesized that the glassy nature of the PGMA below T_g

may cause issues in accessing higher order morphologies.[33] To investigate the validity of this hypothesis PISA3 and PISA6 were heated to 60°C for 12 h post-PISA and the morphological transition was monitored by AFM. Interestingly, this thermal annealing allowed the kinetically trapped, as-prepared aggregates to transition to worm-like micelle and compound (aggregated) nanosphere assemblies for PISA 3 and 6, respectively (Figure 2b and d). For PISA6, some gelation/precipitation was observed leading to the imaging of only MeOH dispersed aggregates via AFM.

One of the most useful aspects of PhotoATRP is the facile ability to perform chain extensions allowing for controlled synthesis of multi-block copolymers with high sequence fidelity and versatility. To apply this to Photo ATR-PISA, sequential chain extensions of the hydrophobic, core-forming PGMA block through successive additions of monomer were attempted (Figure 3a). In between each monomer addition, the UV light used to mediate the PhotoATRP process is shut off for a given time stopping the polymerization reaction, as evidenced by the stable M_n during this time period (Figure 3b and c). This provides evidence for temporal control in the polymerization simply by pulsing UV light over different time periods essentially turning the polymerization off and on.

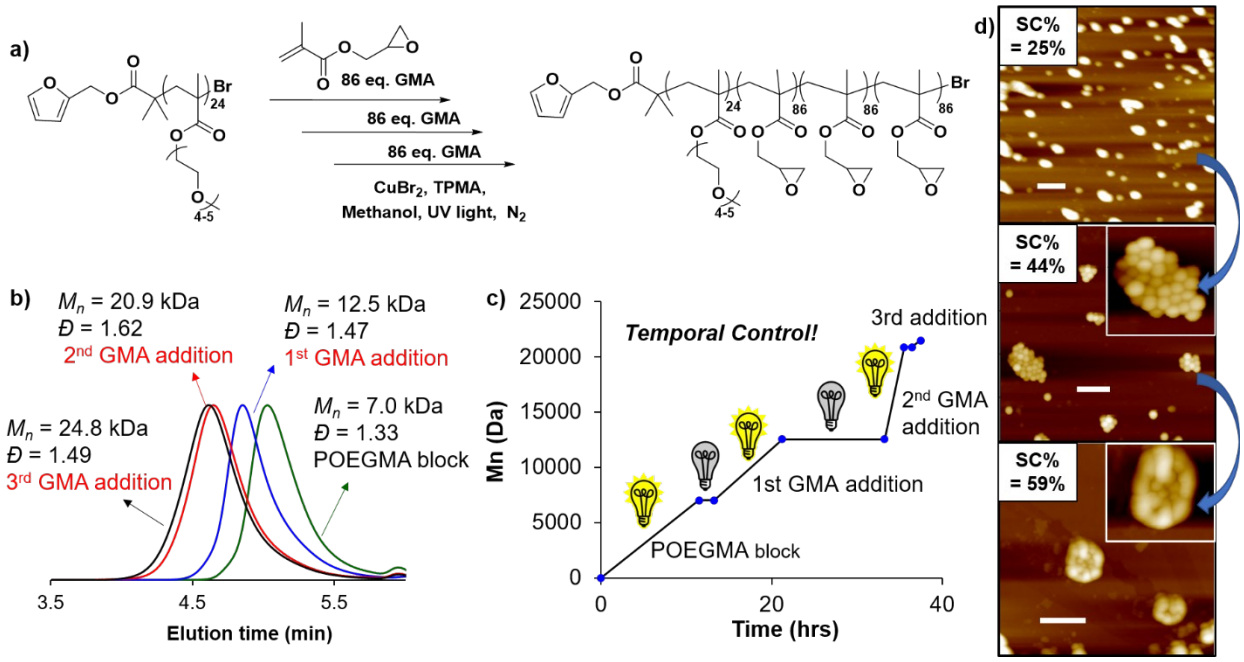

Figure 3. One-pot, PhotoATR-PISA sequential chain extensions from POEGMA macroinitiators allows multiple short segments of PGMA (a and b) to be incorporated successively opening up potential for multi-block copolymer synthesis in PISA with temporal control (c). Upon each addition of GMA monomer, the SC% increases from 25% to 44% to 59% through the three successful chain extensions causing morphological transitions from dispersed nanospheres to compound nanospheres to vesicles as evidenced by AFM (d; white scale bars = 400 nm; inset AFM images = 500 x 500 nm).

GPC analysis upon consumption of monomer following each addition again showed clear increases in M_n with narrow, monomodal peaks indicating successful chain extension until the 4th monomer addition where the polymer nanoparticles become too concentrated and begin to precipitate. This essentially terminates the polymerization quenching the chain extensions at this point. AFM and DLS analysis of the polymer nanostructures formed upon each chain extension

suggested morphological evolution as the polymer M_n and SC% increased. Since additional monomer was added without solvent, the total SC% increased with each addition from 25 w% to 44 w% to 59 w% with the 1st, 2nd, and 3rd additions, respectively. In turn, we were able to identify new nanostructured morphologies upon each sequential monomer addition, transitioning from dispersed nanospheres to compound nanospheres to vesicles with each chain extension and solid content increase (Figure 3d). DLS analysis (Figure S8) showed that the NP hydrodynamic size increased from the first (D_h = 47 nm) to second addition (D_h = 193 nm); how-ever, the NP size became smaller (D_h = 150 nm) following the third chain extension albeit with a broader distribution of NP sizes. We hypothesize that the increase in concentration allowed for the fusion of compound nanospheres forming vesicle aggregate with a range of sizes due the variability of total aggregated nanospheres per compound nanosphere.

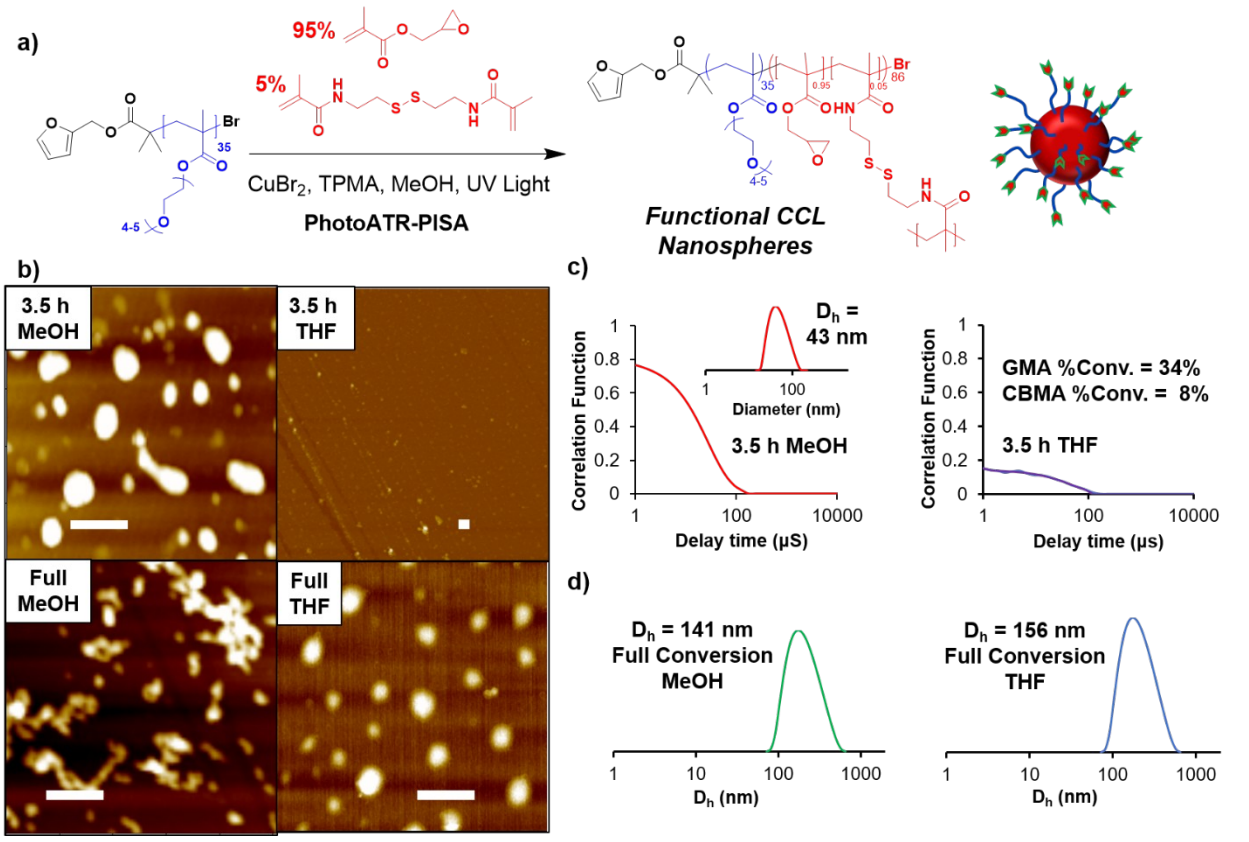

Figure 4. One-pot fabrication of CCL polymer NPs via PhotoATR-PISA of 95% GMA and 5% CBMA allowing for slow incorporation of crosslinks (a). After 3.5 h reaction time where CBMA conversion is only 8%, aggregates are fully dissociated upon switching solvents from MeOH to THF as evidenced by AFM (b; white scale bars = 400 nm) and DLS (c) but, at full conversion, aggregates remain intact showing larger Dh in THF due to swelling of both POEGMA and PGMA (d).

Previously reported kinetic data for RAFT polymerizations suggest that the rate of polymerization for N-(2-hydroxypropyl)methacrylamide is substantially slower than that of 2-dimethylaminoethyl methacrylate due to the lower transfer coefficient reaction of methacrylamide

monomers versus methacrylate monomers.[34-35] Inspired by this, cystamine bismethacrylamide (CBMA) was utilized as the crosslinking agent (Figure 4a). By this method, the CCL process was designed to be delayed until late stages of the polymerization enabling one-pot formation of CCL NPs due to the lower reactivity of CBMA in comparison to GMA. PhotoATR-PISA of GMA and CBMA with the feed molar ratio of CBMA:GMA = 0.05:0.95 were performed at SC% = 25% in methanol (DP(POGEMA) = 35) to in situ CCL NPs all in one-pot (Figure 4; DP(PGMA) = 86, SC% = 25%). ^{1}H NMR analysis at different time intervals was performed to study GMA and CBMA conversion over time (Figure S9). As demonstrated, the crosslinking process was much slower compared to the NPs formation and GMA consumption. For example, after reacting for 3.5 h, the GMA conversion was 34% whereas CBMA conversion was only 8%. Via AFM, we observed the onset of aggregation with nanospheres visible but, after switching to a good solvent like tetrahydrofuran (THF), the NPs were dissolved and no material was detected on the substrate (Figure 4b). This observation was further supported via DLS showing aggregation in MeOH (D_h = 43 nm) with no aggregation observed in THF, as evidenced by the low intensity for the correlation function (Figure 4c). In contrast, at approximately full conversion for both the GMA and CBMA, NPs in both solvents can be observed with mixtures of worms and spheres in MeOH and spheres in THF. Via DLS, the aggregates in THF had larger diameters (Dh = 156 nm) compared to methanol dispersions (Dh= 141 nm) suggesting some unfolding/swelling of polymer chains within the aggregates due to favorable interactions with the THF solvent (Figure 4d).

The installation of disulfide functional CCLs provides potential for stimuli-responsiveness triggered by reduction to free thiols. For this purpose, we attempted to perform NP dissociation experiments with CBMA CCL NPs synthesized by PhotoATR-PISA. Concurrently, with the formation of the NPs, Nile red (0.01% feed molar ratio of GMA) was encapsulated in the NPs during PISA as a fluorescent indicator. Dialysis against water was performed to remove the unencapsulated Nile red at the end of polymerization. AFM and DLS analysis were performed on the resulting NPs (Figures S10). CCL nanosphere were obtained for the sample after dialysis in water, however, some agglomeration of the NPs was observed in the THF, as evidenced by AFM (Figure S10). This is further supported by DLS analysis of these dispersions where we see substantially larger diameters with D_h = 288 nm in THF compared to D_h = 157 nm in water.

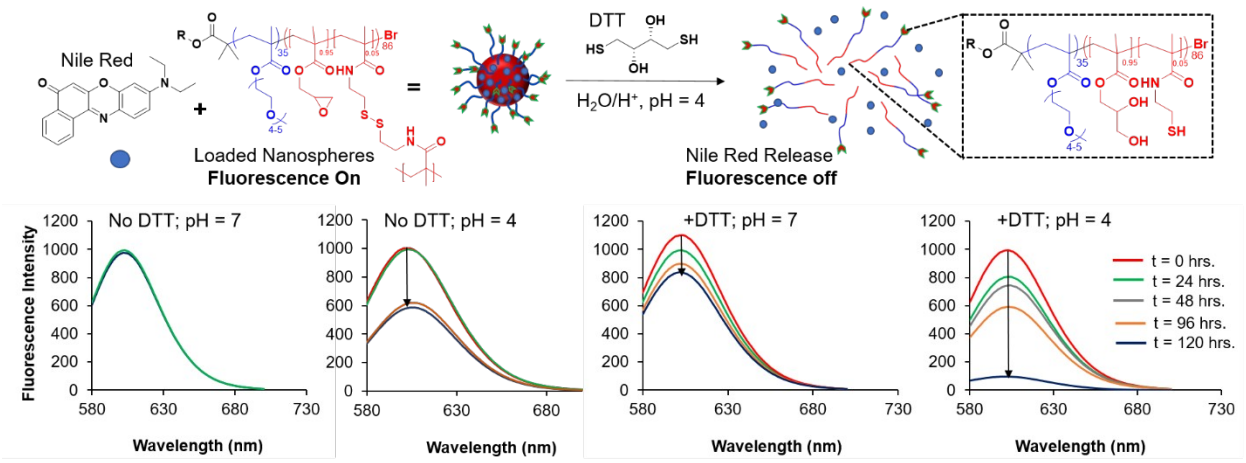

Figure 5. Nile red release via combined DTT reduction of disulfide CCLs and acid-catalyzed hydrolysis of PGMA epoxide pendants causing full dissociation of NPs and release of cargo due to the formation of uncrosslinked hydrophilic copolymers, as evidenced by fluorescence spectroscopy.

The release behavior for the Nile red using dithiothreitol (DTT) as a redox trigger (c = 0.35 M) was investigated. Fluorescence spectra of the NPs with and without DTT and at different pH are shown in Figure 5 (λ_{ex}=540 nm; λ_{em}=630 nm). It is well-known that the Nile red fluorescence is influenced by solvent polarity where emission is red shifted and quenched upon introduction to

polar media.[26, 36] When no DTT is present at neutral pH, the NPs appear to be stable during the 120 h window of monitoring showing no decrease in fluorescence. Upon addition of DTT, we observed a modest decrease in emission intensity over 120 h suggesting some but not all Nile red was released. In contrast, at acidic pH with DTT, the emission intensity of the Nile red decreased to nearly zero, attributed to the full dissolution of NPs and release of Nile red. This is supported further via AFM where only one agglomerated NP was able to be imaged on the substrate (Figure S11). We hypothesize that for release to occur fully, both DTT and acidic pH are required to allow for reduction of the disulfide CCL and ring-opening hydrolysis of the PGMA epoxide pendant group converting these segments to hydrophilic and allowing the copolymers to fully dissolve. It should be noted that at acidic pH without added DTT, we observed decreases in fluorescence intensity to a lesser extent which can be attributed to the hydrolysis of the epoxide pendants without reduction of CCLs allowing water to penetrate into the core of NPs still quenching the fluorescence of Nile red. This is further supported via DLS showing NPs remain intact at acidic pH without DTT (Figure S12), as evidenced by the changes in intensity for the correlation function for the different samples.

Conclusion

In conclusion, the controlled fabrication of polymer NPs using PhotoATR-PISA was accomplished all in one pot starting from POEGMA macroinitiator synthesis to PISA to CCL without any workup. PISA was accomplished at low copper concentration (<20 ppm) and at ambient temperature, demonstrating morphological evolution as a function of SC%, DP(PGMA) and post-polymerization thermal annealing. At SC = 25%, we observe only nanospheres via AFM with observed increases in NP diameter via AFM and DLS as DP(PGMA) increases. At SC% = 32%, the NP morphologies switched to mixtures of worms and spheres. Upon thermal treatment of both PISA samples with DP(PGMA) = 258, the morphologies shifted accessing higher order worm-like micelle or compound nanosphere aggregates exclusively at SC% = 25% and 32%, respectively. Three sequential chain extensions were performed for PGMA shifting the NP morphology upon each addition from nanospheres to compound nanospheres to vesicles, opening potential for multi-block copolymer synthesis in PISA. The CCL procedure was implemented in one pot without any post-treatment and the NPs exhibited increased stability in good solvent like THF. Finally, the responsivity of NPs to redox triggers was investigated showing complete release of cargo only when DTT was present at acidic pH.

Funding Sources

We would like to graciously thank the Massachusetts Technology Transfer Center (MTTC) Acorn Innovation Award and University of Massachusetts Lowell Seed grant for their funding of the described research.

Acknowledgements

We would like to thank all of the UML Core Research Facilities (CRF) staff for their help in data acquisition, most notably Wendy Gavin for her help in NMR analysis and Earl Ada for his help.

References

1. Penfold, N. J. W.; Yeow, J.; Boyer, C.; Armes, S. P., Emerging Trends in Polymerization-Induced Self-Assembly. *ACS Macro Letters* **2019,** *8* (8), 1029-1054.
2. Derry, M. J.; Fielding, L. A.; Armes, S. P., Polymerization-induced self-assembly of block copolymer nanoparticles via RAFT non-aqueous dispersion polymerization. *Progress in Polymer Science* **2016,** *52*, 1-18.
3. Coessens, V. M. C.; Matyjaszewski, K., Fundamentals of Atom Transfer Radical Polymerization. *Journal of Chemical Education* **2010,** *87* (9), 916-919.
4. Warren, N. J.; Armes, S. P., Polymerization-Induced Self-Assembly of Block Copolymer Nano-objects via RAFT Aqueous Dispersion Polymerization. *Journal of the American Chemical Society* **2014,** *136* (29), 10174-10185.
5. Qiao, X. G.; Lansalot, M.; Bourgeat-Lami, E.; Charleux, B., Nitroxide-Mediated Polymerization-Induced Self-Assembly of Poly(poly(ethylene oxide) methyl ether methacrylate-co-styrene)-b-poly(n-butyl methacrylate-co-styrene) Amphiphilic Block Copolymers. *Macromolecules* **2013,** *46* (11), 4285-4295.
6. Anastasaki, A.; Oschmann, B.; Willenbacher, J.; Melker, A.; Van Son, M. H. C.; Truong, N. P.; Schulze, M. W.; Discekici, E. H.; McGrath, A. J.; Davis, T. P.; Bates, C. M.; Hawker, C. J., One-Pot Synthesis of ABCDE Multiblock Copolymers with Hydrophobic, Hydrophilic, and Semi-Fluorinated Segments. *Angewandte Chemie International Edition* **2017,** *56* (46), 14483-14487.
7. Anastasaki, A.; Nikolaou, V.; McCaul, N. W.; Simula, A.; Godfrey, J.; Waldron, C.; Wilson, P.; Kempe, K.; Haddleton, D. M., Photoinduced Synthesis of α,ω-Telechelic Sequence-Controlled Multiblock Copolymers. *Macromolecules* **2015,** *48* (5), 1404-1411.

8. Whitfield, R.; Parkatzidis, K.; Rolland, M.; Truong, N. P.; Anastasaki, A., Tuning Dispersity by Photoinduced Atom Transfer Radical Polymerisation: Monomodal Distributions with ppm Copper Concentration. *Angewandte Chemie International Edition* **2019,** *58* (38), 13323-13328.
9. Allison-Logan, S.; Karimi, F.; Sun, Y.; McKenzie, T. G.; Nothling, M. D.; Bryant, G.; Qiao, G. G., Highly Living Stars via Core-First Photo-RAFT Polymerization: Exploitation for Ultra-High Molecular Weight Star Synthesis. *ACS Macro Letters* **2019,** *8* (10), 1291-1295.
10. Murtezi, E.; Yagci, Y., Simultaneous Photoinduced ATRP and CuAAC Reactions for the Synthesis of Block Copolymers. *Macromolecular Rapid Communications* **2014,** *35* (20), 1782-1787.
11. Yang, Q.; Guerre, M.; Ladmiral, V.; Ameduri, B., Thermal and photo-RAFT polymerization of 2,2,2-trifluoroethyl α-fluoroacrylate. *Polymer Chemistry* **2018,** *9* (24), 3388-3397.
12. Tan, J.; Dai, X.; Zhang, Y.; Yu, L.; Sun, H.; Zhang, L., Photoinitiated Polymerization-Induced Self-Assembly via Visible Light-Induced RAFT-Mediated Emulsion Polymerization. *ACS Macro Letters* **2019,** *8* (2), 205-212.
13. Tan, J.; Huang, C.; Liu, D.; Zhang, X.; Bai, Y.; Zhang, L., Alcoholic Photoinitiated Polymerization-Induced Self-Assembly (Photo-PISA): A Fast Route toward Poly(isobornyl acrylate)-Based Diblock Copolymer Nano-Objects. *ACS Macro Letters* **2016,** *5* (8), 894-899.
14. Tan, J.; Sun, H.; Yu, M.; Sumerlin, B. S.; Zhang, L., Photo-PISA: Shedding Light on Polymerization-Induced Self-Assembly. *ACS Macro Letters* **2015,** *4* (11), 1249-1253.
15. Xu, S.; Corrigan, N.; Boyer, C., Forced gradient copolymerisation: a simplified approach for polymerisation-induced self-assembly. *Polymer Chemistry* **2020**, Ahead of Print, DOI: 10.1039/D0PY00889C.
16. Hatton, F. L.; Lovett, J. R.; Armes, S. P., Synthesis of well-defined epoxy-functional spherical nanoparticles by RAFT aqueous emulsion polymerization. *Polymer Chemistry* **2017,** *8* (33), 4856-4868.
17. Liu, Z.; Zhang, G.; Wei, l.; Huang, Y.; Zhang, J.; Chen, T., UV light-initiated RAFT polymerization induced self-assembly. *Polym. Chem.* **2015,** *6*.
18. Shi, B.; Zhang, H.; Liu, Y.; Wang, J.; Zhou, P.; Cao, M.; Wang, G., Development of ICAR ATRP–Based Polymerization-Induced Self-Assembly and Its Application in the Preparation of Organic–Inorganic Nanoparticles. *Macromolecular Rapid Communications* **2019,** *40* (24), 1900547.
19. Liu, C.; Hong, C.-Y.; Pan, C.-Y., Polymerization Techniques in Polymerization-Induced Self-Assembly (PISA). *Polymer Chemistry* **2020,** *11*.
20. Docherty, P. J.; Derry, M. J.; Armes, S. P., RAFT dispersion polymerization of glycidyl methacrylate for the synthesis of epoxy-functional block copolymer nanoparticles in mineral oil. *Polymer Chemistry* **2019,** *10* (5), 603-611.

21. Blanazs, A.; Ryan, A. J.; Armes, S. P., Predictive Phase Diagrams for RAFT Aqueous Dispersion Polymerization: Effect of Block Copolymer Composition, Molecular Weight, and Copolymer Concentration. *Macromolecules* **2012,** *45* (12), 5099-5107.
22. Liu, D.; Zeng, R.; Sun, H.; Zhang, L.; Tan, J., Blue Light-Initiated Alcoholic RAFT Dispersion Polymerization of Benzyl Methacrylate: A Detailed Study. *Polymers* **2019,** *11*, 1284.
23. Hu, X.; Li, H.; Luo, S.; Liu, T.; Jiang, Y.; Liu, S., Thiol and pH dual-responsive dynamic covalent shell cross-linked micelles for triggered release of chemotherapeutic drugs. *Polymer Chemistry* **2013,** *4* (3), 695-706.
24. Read, E. S.; Armes, S. P., Recent advances in shell cross-linked micelles. *Chemical Communications* **2007,** (29), 3021-3035.
25. Wang, G.; Schmitt, M.; Wang, Z.; Lee, B.; Pan, X.; Fu, L.; Yan, J.; Li, S.; Xie, G.; Bockstaller, M. R.; Matyjaszewski, K., Polymerization-Induced Self-Assembly (PISA) Using ICAR ATRP at Low Catalyst Concentration. *Macromolecules* **2016,** *49* (22), 8605-8615.
26. Wang, C.; Wang, Z.; Zhang, X., Amphiphilic Building Blocks for Self-Assembly: From Amphiphiles to Supra-amphiphiles. *Accounts of Chemical Research* **2012,** *45* (4), 608-618.
27. Cao, M.; Zhang, Y.; Wang, J.; Fan, X.; Wang, G., ICAR ATRP Polymerization-Induced Self-Assembly Using a Mixture of Macroinitiator/Stabilizer with Different Molecular Weights. *Macromolecular Rapid Communications* **2019,** *40* (20), 1900296.
28. Pan, X.; Malhotra, N.; Simakova, A.; Wang, Z.; Konkolewicz, D.; Matyjaszewski, K., Photoinduced Atom Transfer Radical Polymerization with ppm-Level Cu Catalyst by Visible Light in Aqueous Media. *Journal of the American Chemical Society* **2015,** *137* (49), 15430-15433.
29. Wang, Z.; Pan, X.; Yan, J.; Dadashi-Silab, S.; Xie, G.; Zhang, J.; Wang, Z.; Xia, H.; Matyjaszewski, K., Temporal Control in Mechanically Controlled Atom Transfer Radical Polymerization Using Low ppm of Cu Catalyst. *ACS Macro Letters* **2017,** *6* (5), 546-549.
30. Chantasirichot, S.; Inoue, Y.; Ishihara, K., Photoinduced atom transfer radical polymerization in a polar solvent to synthesize a water-soluble poly(2-methacryloyloxyethyl phosphorylcholine) and its block-type copolymers. *Polymer* **2015,** *61*, 55-60.
31. Tsarevsky, N. V.; Pintauer, T.; Matyjaszewski, K., Deactivation Efficiency and Degree of Control over Polymerization in ATRP in Protic Solvents. *Macromolecules* **2004,** *37* (26), 9768-9778.
32. Jia, X.; Listak, J.; Witherspoon, V.; Kalu, E. E.; Yang, X.; Bockstaller, M. R., Effect of Matrix Molecular Weight on the Coarsening Mechanism of Polymer-Grafted Gold Nanocrystals. *Langmuir* **2010,** *26* (14), 12190-12197.
33. Cheng, D.; Wei, P.; Zhang, L.; Cai, J., Surface-initiated atom transfer radical polymerization grafting from nanoporous cellulose gels to create hydrophobic nanocomposites. *RSC Advances* **2018,** *8* (48), 27045-27053.

34. Chen, M.; Li, J.-W.; Zhang, W.-J.; Hong, C.-Y.; Pan, C.-Y., pH- and Reductant-Responsive Polymeric Vesicles with Robust Membrane-Cross-Linked Structures: In Situ Cross-Linking in Polymerization-Induced Self-Assembly. *Macromolecules* **2019,** *52* (3), 1140-1149.
35. Qu, Q.; Liu, G.; Lv, X.; Zhang, B.; An, Z., In Situ Cross-Linking of Vesicles in Polymerization-Induced Self-Assembly. *ACS Macro Letters* **2016,** *5* (3), 316-320.
36. Sackett, D. L.; Wolff, J., Nile red as a polarity-sensitive fluorescent probe of hydrophobic protein surfaces. *Anal Biochem* **1987,** *167* (2), 228-34.